Evidence for a persistent and extensive greening trend in Eurasia inferred from satellite vegetation index data

J. Bogaert,[1,2] L. Zhou,[1] C. J. Tucker,[3] R. B. Myneni,[1] and R. Ceulemans[4]

[1]   The northern latitudes have warmed by ~0.8°C since the early 1970s, but not all areas have warmed equally. Eurasia shows an overall warming trend, while North America exhibits warming at a lower rate and even a slight cooling trend during the last 50 years in the eastern United States. We analyzed a recently developed satellite normalized difference vegetation index (NDVI) data set (July 1981 to December 1999) to assess vegetation response to these temperature changes. An index of persistence of the NDVI trend was used to generate patches of different levels of persistence. The persistence data were analyzed for patch area, patch perimeter, patch number, patch coherence, largest patch size, patch fragmentation, pixel contiguity, pixel clustering, and conditional probability of pixel adjacency. We address two questions: (1) Is there a difference in the spatial pattern of long-term NDVI increase in comparison to short-term increase? and (2) Are there differences in the spatial patterns of patches between Eurasia and North America? The results indicate a persistent and spatially extensive and connected greening trend in Eurasia, relative to North America. The regions showing short-term greening in Eurasia show a scattered pattern of spatially remote small patches. In North America the long-term greening pattern is spatially fragmented, and a mixture of short- and long-term NDVI increase is found, unlike in Eurasia. Therefore we conclude that the greening trend in Eurasia is more persistent and spatially extensive than in North America, which is qualitatively consistent with near-surface air temperature observations.   *INDEX TERMS:* 1640 Global Change: Remote sensing; 1620 Global Change: Climate dynamics (3309); 1851 Hydrology: Plant ecology; *KEYWORDS:* NDVI, global warming, greening, spatial pattern, AVHRR

1.   Introduction

[2]   The effect of climate change on ecosystems, in particular the consequences of temperature increase on plant and animal life, is a topic of paramount importance. Analysis of temperature records from meteorological stations shows unprecedented rate of temperature change during the past 25 years [*Hansen et al.*, 1999]. The northern latitudes experienced enhanced warming, especially during the winter and spring periods. The biotic response to warming can be assessed in multiple ways, e.g., phenological changes in plants [*Myneni et al.*, 1997; *Colombo*, 1998; *Schwartz*, 1998; *Bradley et al.*, 1999; *Menzel and Fabian*, 1999; *Cayan et al.*, 2001; *Fitzjarrald et al.*, 2001; *Zhou et al.*, 2001] and changes in animal behavior [*Crick et al.*, 1997; *Brown et al.*, 1999; *Crick and Sparks*, 1999; *Parmesan et al.*, 1999; *Thomas and Lennon*, 1999].

[1]Department of Geography, Boston University, Boston, Massachusetts, USA.

[2]On leave from Department of Biology, University of Antwerp, Wilrijk, Belgium.

[3]Biospheric Sciences Branch, NASA Goddard Space Flight Center, Greenbelt, Maryland, USA.

[4]Department of Biology, University of Antwerp, Wilrijk, Belgium.

[3]   Analyses of satellite-measured vegetation index data suggest increased photosynthetic activity in a manner associated with an increase in the length of the active growing season in the northern high latitudes [*Myneni et al.*, 1997; *Zhou et al.*, 2001]. This has implications for the global carbon cycle. An increase in the amplitude of the seasonal CO_2 cycle in the Northern Hemisphere since the early 1960s has been detected [*Keeling et al.*, 1996] and related to northern vegetation activity [*Randerson et al.*, 1999].

[4]   Spatially averaged normalized difference vegetation index (NDVI) and near-surface air temperature anomalies are shown in Figure 1a for vegetated regions in the 40°N–70°N band [*Zhou et al.*, 2001]. The correlation between satellite NDVI and station temperature changes in both Eurasia and North America suggests a possible vegetation response to warming. The NDVI data capture the contrast between red and near-infrared reflectance of vegetation, which signals the abundance and energy absorption by chlorophyll. Thus the NDVI data are generally well correlated with the fraction of photosynthetically active radiation absorbed by vegetation [e.g., *Asrar et al.*, 1984; *Myneni et al.*, 1995, 1997]. This concept underlies the use of NDVI as a proxy for monitoring photosynthetic activity on a global scale [*Tucker et al.*, 1985, 1986].

[5]   A pattern of NDVI change distinct between Eurasia and North America was noted by *Zhou et al.* [2001] based on the same 18.5-year record. They report that North
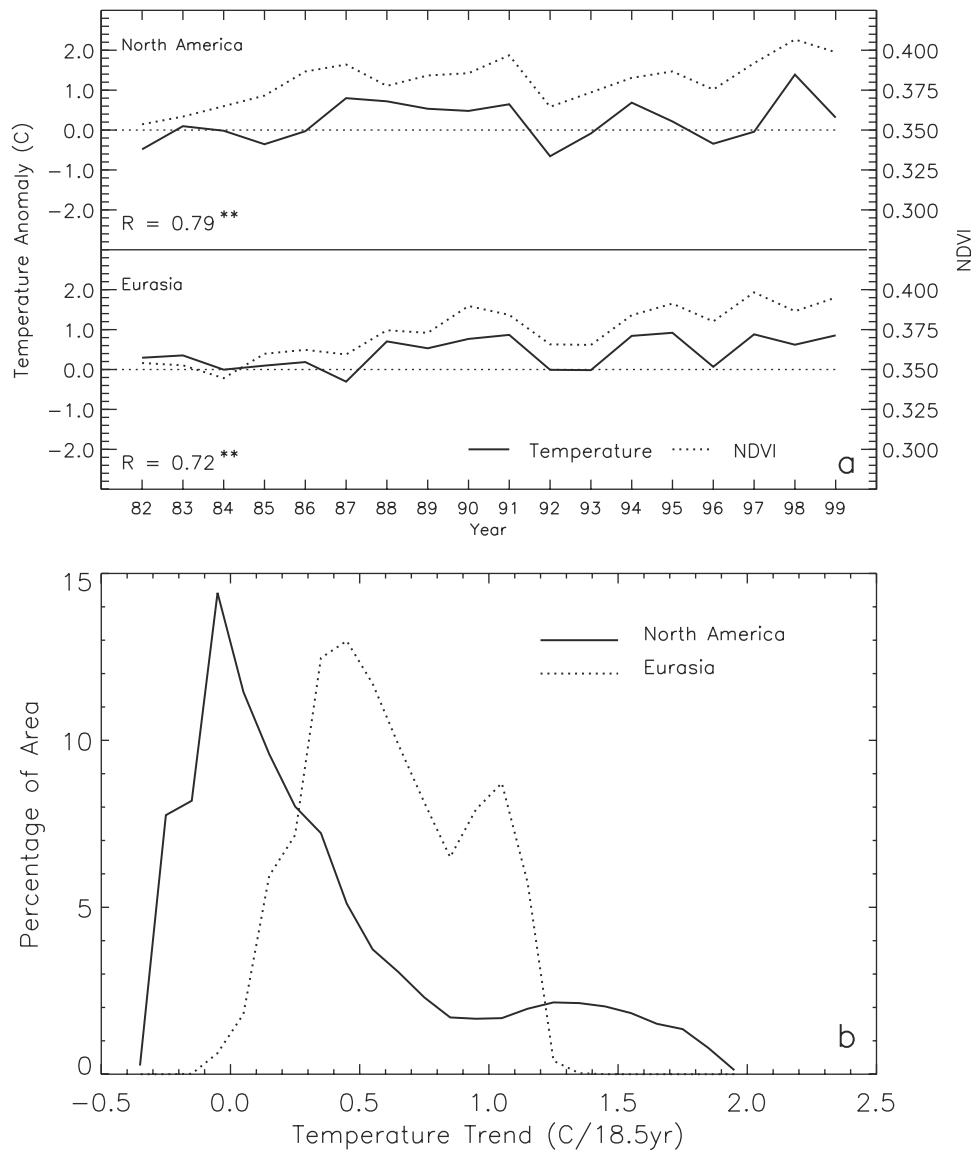
Figure 1. Indications of temperature and normalized difference vegetation index (NDVI) increase in the northern latitudes. (a) Spatially averaged NDVI and near-surface air temperature anomaly between 40°N and 70°N for the growing season (April–October) for an 18.5-year record (July 1981 to December 1999). *R* is the correlation coefficient; the double asterisk denotes statistical significance at the 0.01 level [*Zhou et al.*, 2001]. (b) Fraction of vegetated area in North America and Eurasia subjected to temperature increase or decrease, calculated for an 18.5-year record (July 1981 to December 1999) and for the growing season (April–October) between 20°N and 80°N.

America shows a fragmented pattern of change in smaller areas while Eurasia exhibits a persistent increase in growing season NDVI over a broad contiguous swath of land. Analysis of the distribution of vegetated area by temperature trends confirms the findings of *Zhou et al.* [2001] (Figure 1b). North America shows a skewed distribution of temperature change with a larger fractional area under a marginal cooling trend that is hardly compensated by the area under intensive warming. Eurasia, on the other hand, shows mostly a warming trend with negligible occurrence of cooling. *Zhou et al.* [2001] characterized the consistency of NDVI trends in terms of a persistence index and draw these conclusions from a cursory analysis of the areal extent of trends at different persistence levels. Trends based on short record lengths must

necessarily be interpreted with caution. The spatial patterns of temporal changes in NDVI provide information that potentially can enhance confidence in the observed trends. Trends that show spatial proximity and coherence are more reliable than those observed only in spatially fragmented regions because the patterns are indicative of the underlying cause for change. The argument of *Zhou et al.* [2001] that NDVI changes are spatially different between Eurasia and North America thus raises two questions. First, what are the differences in the spatial pattern of regions exhibiting short-term NDVI increase in comparison to regions showing long-term increase? Second, what are the differences in the spatial pattern between Eurasia and North America of regions showing a long-term NDVI increase? These issues are

addressed in this article mainly with methods developed in landscape ecology [*Fortin*, 1999], a branch of science developed to analyze ecological processes in their spatial context [e.g., *Antrop*, 2001; *Stine and Hunsaker*, 2001].

[6] Landscape ecology is based on the premise that there are strong links between patterns, functions and processes [*Gustafson*, 1998]. A number of studies have explored the utility of spatial metrics in landscape analysis since the 1980s [e.g., *Krummel et al.*, 1987; *O'Neill et al.*, 1988; *Turner*, 1989; *Ripple et al.*, 1991; *Haines-Young and Chopping*, 1996; *Schumaker*, 1996; *Bogaert et al.*, 1999; *He et al.*, 2000; *Bogaert et al.*, 2001]. A set of indices is frequently evaluated because no single metric fully captures the complexity of the spatial arrangement of patches. As a result, the number of indices has proliferated, many of which have been shown either to be correlated [*Riiters et al.*, 1995; *Hargis et al.*, 1998; *Bogaert et al.*, 1999] or to exhibit statistical interactions with one another [*Li and Reynolds*, 1994]. There have been attempts to develop metrics that combine multiple components of a pattern into a single value [*Bogaert et al.*, 2000c]. On the other hand, the use of statistical methods such as factor analysis to reduce the number of indices [*Riiters et al.*, 1995; *Cain et al.*, 1997; *Bogaert et al.*, 1999; *Herzog et al.*, 2001] does not render the ecological meaning of a metric to the analyst [*Riiters et al.*, 1995]. Generally, one should attempt to describe independent and fundamental components of a spatial pattern by utilizing a suite of metrics [*Li and Reynolds*, 1994; *Riiters et al.*, 1995; *Giles and Trani*, 1999]. Therefore, in the present study we use patch size coherence [*Jaeger*, 2000], pixel contiguity and clustering [*LaGro*, 1991], neighborship probability [*Riiters et al.*, 2000], and indices of largest patch [*McGarigal and Marks*, 1995] and fragmentation [*Johnsson*, 1995], in addition to basic patch statistics of area, perimeter, and number, to study the spatial structure of NDVI trends in the northern latitudes.

2. Data Set and Methods

2.1. GIMMS NDVI Data Set

[7] A global data set at 8-km resolution (square pixels) developed by the Global Inventory Monitoring and Modeling Studies (GIMMS) group was used in this study. The data are from the Advanced Very High Resolution Radiometers (AVHRR) onboard the NOAA series satellites (NOAA 7, 9, 11, and 14) and cover the period July 1981 to December 1999. The data set contains channels 1 (0.58–0.68 μm) and 2 (0.73–1.1 μm) reflectances, channels 4 (10.3–11.3 μm) and 5 (11.5–12.5 μm) brightness temperatures, solar and view zenith angles, and the day of compositing. All data correspond to the maximum NDVI value during a 15-day composite period ($|NDVI| \leq 1$). The NDVI values are about −0.2 to 0.1 for snow, inland water bodies, deserts, exposed soils, and sparsely vegetated areas and increase from 0.1 to ∼0.7 for increasing amounts of vegetation.

[8] The satellite data processing included improved navigation, sensor calibration, and improved atmospheric corrections. The data navigation algorithm used an accurate orbital model, latest satellite ephemeris information and instrument clock correction in addition to a digital elevation model to account for target elevation [*Rosborough et al.*, 1994]. A technique based on data from high cold clouds and dark ocean was used to calibrate the data set [*Vermote and*

Kaufman, 1995]. This calibration was deemed insufficient and improved by a method developed by *Los* [1998]. The data for the periods April 1982 to December 1984 and June 1991 to December 1993 were corrected to remove the effects of stratospheric aerosol loading from El Chicon and Mount Pinatubo eruptions [*Vermote and El Saleous*, 1994]. Residual atmospheric effects were minimized by analyzing only the maximum NDVI value within each 15-day compositing period; days 1 to 15 form the first interval, and days 16 to the end of the month the second. These data generally correspond to observations in the forward, nearest to near-nadir view directions [*Los et al.*, 1994] and clear atmospheres [*Holben*, 1986]. Bidirectional effects and residual atmospheric effects are, however, not fully eliminated by this approach. Further technical discussion on the quality of AVHRR vegetation index data can be found in the works of *Kaufmann et al.* [2000] and *Zhou et al.* [2001].

[9] Only vegetated pixels were analyzed to further reduce any remaining nonvegetation effects on the data and to exclude snow, barren, and sparsely vegetated areas. Vegetated regions were delineated as those with (1) June to August NDVI composite values exceeding 0.1 in all years; and (2) June to August average NDVI value exceeding 0.3 in all years [*Zhou et al.*, 2001]. The 8-km resolution data were aggregated to a $0.25° \times 0.25°$ resolution to reduce computational burden.

[10] The persistence index (*PI*) as defined by *Zhou et al.* [2001] was used to illustrate spatial occurrence of NDVI changes during the growing season. Linear trends in growing season average NDVI were calculated for the periods 1982–1987, 1982–1989, 1982–1991, 1982–1993, 1982–1995, 1982–1997, and 1982–1999. These trends are denoted as $t(i)$, with $i = 1, ..., 7$. A score of 1 is assigned if $t(i + 1) > 0.8$ $t(i)$; otherwise, a score of 0 is given. The sum of these scores is defined as *PI*; thus $0 \leq PI \leq 6$. Regions can therefore be identified where NDVI has increased consistently based on the *PI*. The higher the *PI*, the longer the period a pixel shows increase of NDVI. The analysis was restricted to pixels with $PI \geq 2$ and to vegetated areas in the latitudinal band 20°N to 80°N.

[11] Pixels were aggregated into "patches" based on orthogonal pixel neighborships for each persistence level (Figure 2). Two pixels are grouped in one patch if they are orthogonal neighbors ("nearest" neighbors). Orthogonal neighbors are also denoted as "adjacent". Two pixels that are diagonal neighbors ("next-nearest" neighbors) belong to the same patch if they are connected through other pixels with orthogonal neighborships. A threshold of 9 pixels was used in the patch-level analysis because patches composed of small numbers of pixels constrain pattern quantification [*Milne*, 1991; *O'Neill et al.*, 1999]. Thus this study describes a patch-level analysis to assess spatial patterning of NDVI increase instead of pixel-level analysis, which is typical of most remote sensing studies [e.g., *Myneni et al.*, 1997; *Zhou et al.*, 2001]. Patch mosaics constitute another perception of the spatial structure of the data in which data within patches are defined as spatially homogeneous entities and in which spatial arrangement among patches is of interest [*Fortin*, 1999].

2.2. Evenness as a Measure of Variability of Index Values

[12] We use the concept of evenness to compare variability of the indices (see section 2.3) between Eurasia and
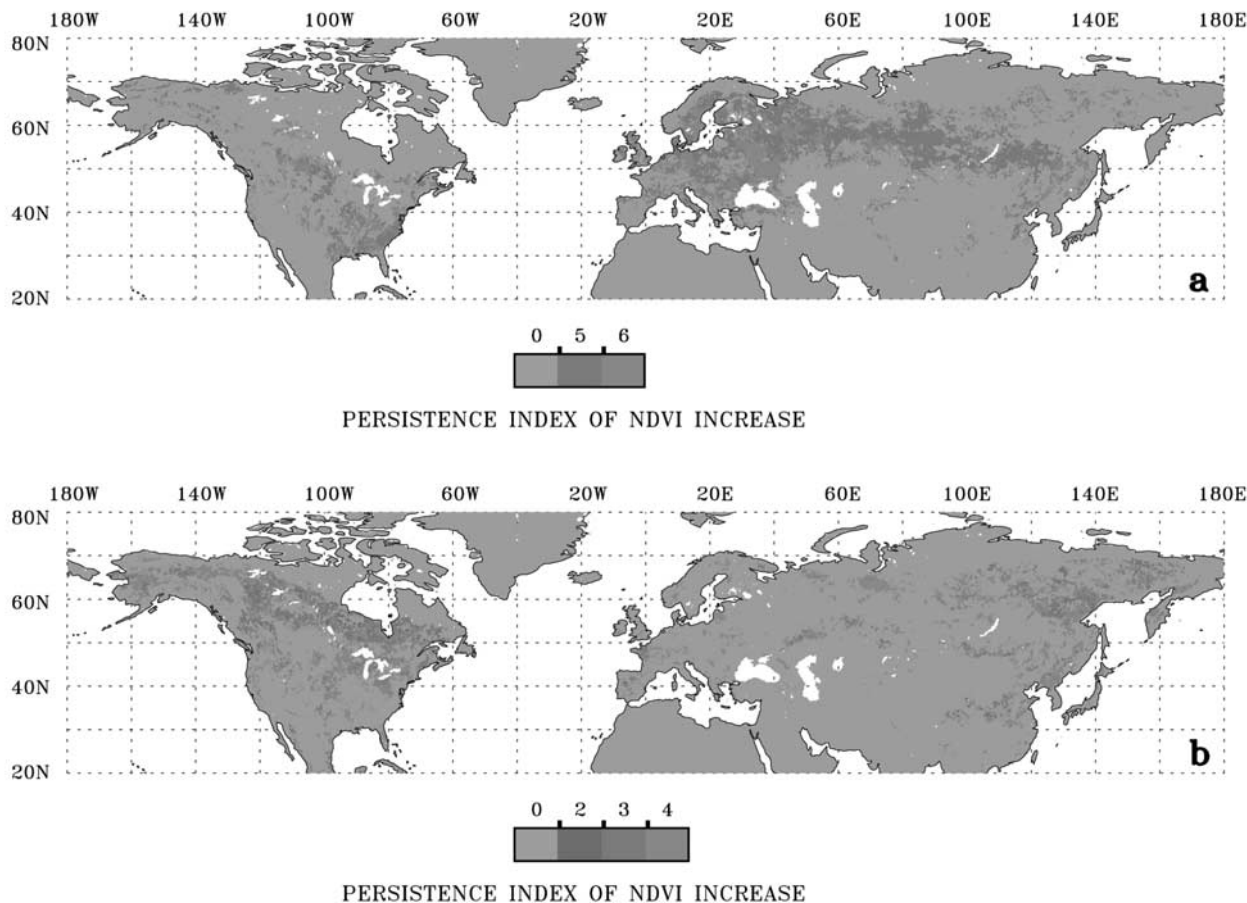
Figure 2. Spatial presence of persistent NDVI increase in the northern latitudes. (a) Zones of long-term greening, characterized by five or six periods of growing season average NDVI increase. (b) Zones of short-term greening, characterized by less than five periods of growing season average NDVI increase. For spatial analysis, adjacent pixels representing an identical persistence index value are clustered into "patches." See color version of this figure at back of this issue.

North America and between low and high persistence values. Higher evenness in this context indicates that the index outcomes are closer to one another; lower evenness, also denoted as "dominance", indicates otherwise. The length of the Lorenz curve is used to assess evenness [*Lorenz*, 1905; *Rousseau et al.*, 1999]. The outcomes are ranked from low to high, replacing their values by their relative proportion, and using the sum of all values. The data are thus transformed into a cumulative series. If v_i represents the ith value of a ranked series of z values ($v_i \geq v_{i-1}$; $z \geq i$; $z, i \in \mathbb{N}$), v_i is hence replaced by v_i^*,

$$v_i^* = \frac{1}{v_t} \sum_{j=1}^{i} v_j, \tag{1}$$

where $v_t = v_1 + v_2 + \ldots + v_z$ and $v_i^* \geq v_{i-1}^*$. To construct the corresponding Lorenz curve, every v_i^* value is plotted on the ordinate against its rank number, divided by the total number of values (= i/z) on the abscissa. The length of

the Lorenz curve L can be derived from the graph and is calculated as [*Bogaert et al.*, 2000b]

$$L = \sum_{i=1}^{z} \sqrt{\frac{1}{z^2} + \left(v_i^* - v_{i-1}^*\right)^2} = \sum_{i=1}^{z} \sqrt{\frac{1}{z^2} + \left(\frac{v_i}{v_t}\right)^2}. \tag{2}$$

In case of perfect evenness, i.e., $\forall i, j \leq z : v_i = v_j$, the curve coincides with the diagonal (1:1 line) and $L = \sqrt{2}$, because both abscissa and ordinate have a length equal to one ($v_z^* = 1$). For a data series characterized by high dominance, i.e., $\exists! \; i \neq j: v_i \gg v_j, L \approx 2$. Higher L values hence indicate higher variation within the data series. Evenness is at best expressed as a partial order [*Rousseau et al.*, 1999] and is thus adequately represented by a Lorenz curve [*Taillie*, 1979]. The order is not total because the curves can cross each other in which case evenness cannot be used for they can generate identical L values [*Bogaert et al.*, 2000b].

2.3. Spatial Pattern Metrics

[13] The main properties of planar shapes are area and perimeter [*Bribiesca*, 1997]. Patch area can be expressed in
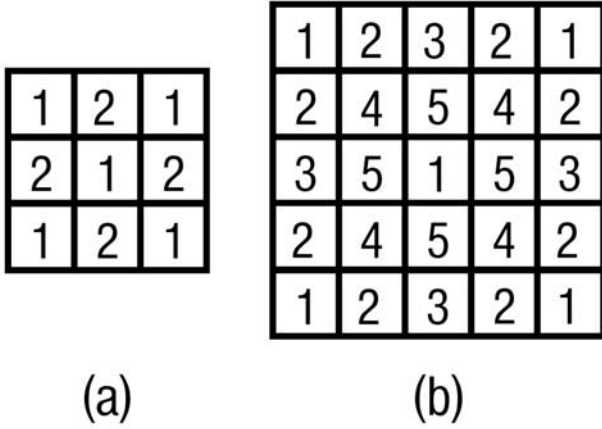
Figure 3. Spatial pattern metrics: (a) 3×3 template to calculate pixel contiguity G_1 and (b) 5×5 template to calculate pixel clustering G_2.

two ways: by the pixel number or by the actual area represented by the pixel cluster or patch. In our equal angle data set, pixel size is dependent on latitude. The pixel size s_θ at latitude θ is given by

$$s_\theta = \left(\frac{0.25 R \pi}{180}\right)^2 \cos \theta, \qquad (3)$$

with $R = 6.371 \times 10^6$ m, the radius of the Earth. The patch area is the sum of the pixel areas s_θ. Classic perimeter formulas [*Bribiesca*, 1997; *Bogaert et al.*, 2000a] are not applicable because of varying pixel size. Therefore we define patch perimeter as the sum of the adjusted pixel side lengths forming the outer boundary of a patch.

[14] Patch coherence C measures the degree of partitioning of one continuous area into several smaller fractions [*Jaeger*, 2000]. C is calculated as

$$C = \sum_{i=1}^{n} \left(\frac{a_i}{a_t}\right)^2, \qquad (4)$$

where a_i is the area of the ith patch, a_t the total area, n the number of patches considered, and $0 \leq C \leq 1$. Higher

values of C result when a few, large patches are present; the occurrence of many small patches will cause low values of C. The degree of coherence can also be considered as a measure of patch size evenness, i.e., C quantifies the partitioning of a_t over n patches. Perfect evenness is observed if all patches have an equal area, i.e., $\forall i, j: a_i = a_j$. Perfect unevenness or dominance is observed when one single patch has a large area and all others have a minimum area. To show the relationship between L and C, equation (4) can be rewritten as

$$C = c_1 + c_2 + \ldots + c_n, \qquad (5)$$

with c_i equal to $(a_i/a_t)^2$. Analogously, using a_i as substitute for v_i, equation (2) is reformulated as

$$L = \sum_{i=1}^{n} \sqrt{\frac{1}{n^2} + \left(\frac{a_i}{a_t}\right)^2} = l_1 + l_2 + \cdots + l_n. \qquad (6)$$

Consequently, the relationship between L and C is given by

$$l_i = \sqrt{\frac{1}{n^2} + c_i}. \qquad (7)$$

High c_i values, generating a high overall degree of coherence, will cause an increase of the corresponding l_i values which result in longer Lorenz curve lengths, reflecting unevenness of patch area distribution. Coherence measures the tendency of pixels to aggregate in large clusters and hence will increase when large differences of a_i are present. For perfect evenness, $(\forall c_i: c_i = n^{-2})$, $C = n^{-1}$.

[15] The largest patch index S was calculated to assess the fractional area occupied by the largest patch in each data layer [*McGarigal and Marks*, 1995], thus relating the patch area to the total area of the persistence level,

$$S = \frac{a_{\max}}{a_t}, \qquad (8)$$

with $a_{\max}$ the largest patch area observed, i.e., $\forall i: a_i \leq a_{\max}$. High values of S are associated with data layers dominated by one single large patch.

Table 1. Patch Number and Area Statistics[a]

PI	n	a_t km^2	n/a_t, 10^{-5} km^{-2}	$\bar{a}$, km^2	$a_{\max}$ km^2	C.V.
			Eurasia			
2	10	59,241	16.88	5,924	7,367	0.267
3	92	864,802	10.64	9,400	98,698	1.231
4	292	3,468,074	8.42	11,877	194,906	1.603
5	258	8,937,630	2.89	34,642	3,724,820	7.035
6	103	1,671,698	6.16	16,230	392,067	2.494
			North America			
2	50	385,303	12.97	7,706	39,982	0.750
3	89	1,242,232	7.16	13,958	165,418	1.597
4	150	2,350,342	6.38	15,669	187,223	1.699
5	102	2,645,420	3.86	25,935	548,311	2.660
6	41	553,940	7.40	13,511	43,932	0.800

[a] Patch number and area statistics for persistence index (PI) data in Eurasia and North America. Number of patches (n), total area (a_t), patch density (n/a_t), mean patch area ($\bar{a}$), maximum patch area ($a_{\max}$), and the coefficient of variation (C.V.) are listed.
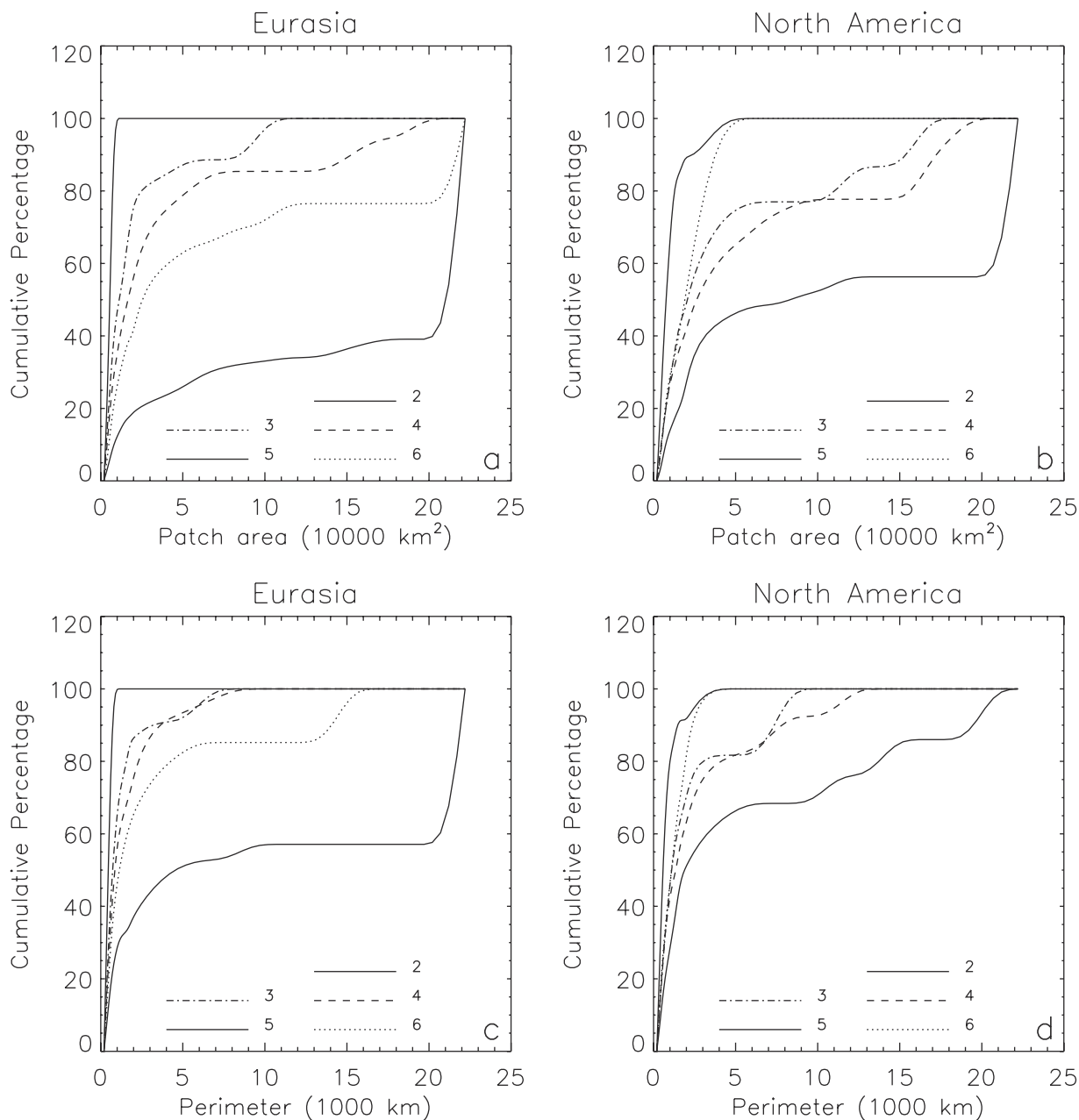
Figure 4. Patch area and perimeter distributions. (a) Cumulative patch size distribution for different persistence values (PI = 2, 3, ..., 6) in Eurasia. (b) Cumulative patch size distribution for different persistence values (PI = 2, 3, ..., 6) in North America. The curves in Figures 4a and 4b represent the proportion of the total area in the data layer that is covered by patches of a particular size. (c) Cumulative patch perimeter distribution for different persistence values (PI = 2, 3, ..., 6) in Eurasia. (d) Cumulative patch perimeter distribution for different persistence values (PI = 2, 3, ..., 6) in North America. The curves in Figures 4c and 4d represent the proportion of the total boundary length in the data layer that is taken by patches with a particular perimeter.

[16] The fragmentation index F measures the aggregation of pixels into patches and is considered as a measure of image complexity [*Johnsson*, 1995]. F is calculated as

$$F = \frac{n-1}{m-1}, \qquad (9)$$

with n the number of patches ($n \geq 1$), m the number of pixels considered, and $0 \leq F \leq 1$. Increasing degrees of fragmentation, i.e., the occurrence of a higher number of

spatially separated pixel clusters, will result in higher values of the fragmentation index. $F = 0$ is measured in the case of one single patch, regardless of its area. Considering that a threshold value of 9 pixels was used in our analysis (section 2.1), the maximum value (F_{max}) is observed for $n = m/9$ and is for $m \gg 1$ equal to

$$F_{max} = \frac{m-9}{9(m-1)} = \frac{n-1}{9n-1} \approx 0.11. \qquad (10)$$

Table 2. Perimeter Statistics[a]

PI	p_t, km	$\bar{p}$, km	p_{max}, km	C.V.
		Eurasia		
2	5,279	528	730	0.284
3	68,014	739	6,217	0.965
4	243,405	834	7,758	1.004
5	417,054	1,616	122,802	4.977
6	102,267	993	15,176	1.635
		North America		
2	32,105	642	2,769	0.614
3	86,257	969	8,059	1.225
4	155,233	1,035	11,778	1.336
5	144,595	1,418	20,208	1.867
6	36,680	895	2,897	0.704

[a] Perimeter statistics for persistence index (PI) data in Eurasia and North America. Total perimeter (p_t), mean patch perimeter ($\bar{p}$), maximum patch perimeter (p_{max}), and the coefficient of variation (C.V.) are listed.

Note that (1) equation (9) has no solution if $m = 1$ and (2) F is measured using pixel counts instead of actual patch and pixel areas based on equation (3), as for C and S.

[17] Assessing the spatial connectedness or contiguity G_1 of cells within a grid cell data set provides information on the overall spatial structure [*LaGro*, 1991]. Contiguity is quantified by convolving a 3×3 pixel template, or mask, with a binary digital image in which the pixels within the class of interest are assigned a value of 1 and the background pixels a value of 0. A template value of 2 is assigned to quantify horizontal and vertical relationships and a value of 1 is assigned to quantify diagonal relationships with the central pixel (Figure 3a). Orthogonally contiguous pixels are consequently more heavily weighted than diagonally contiguous pixels. The value of each pixel in the output image $G_1(i, j)$, computed when at the center of the mask, equals the sum of the products of each template value and the corresponding input pixel value $\gamma(k, l)$, within the nine-cell pixel neighborhood, i.e.,

$$G_1(i,j) = \sum_{k=i-1}^{i+1} \sum_{l=j-1}^{j+1} \tau\gamma(k,l), \qquad (11)$$

with τ the template value dependent on $\varsigma = |i - k| + |j - l|$:

$$\tau = \begin{cases} 1 \Leftrightarrow (\varsigma = 0) \vee (\varsigma = 2) \\ 2 \Leftrightarrow \varsigma = 1 \end{cases}$$

where $\vee$ denotes that one of both conditions should apply. Consequently, $1 \leq G_1(i, j) \leq 13$. The occurrence of large patches will go together with observing the highest pixel contiguity values.

[18] Characterizing the spatial clustering G_2 of pixels provides information on the spatial pattern not provided by assessment of contiguity [*LaGro*, 1991]. A pixel neighborhood of 5×5 pixels is applied to detect, in the vicinity of each image pixel, the presence of nearby noncontiguous pixels of the class being analyzed. Sensitivity to clustering of both contiguous and noncontiguous pixels is achieved by decreasing the template values outward from the central pixel (Figure 3b). For any given pixel, G_2 reflects the pixel's proximity to other pixels within the same class. By

analogy with contiguity the clustering value of each pixel in the output image $G_2(i, j)$ is calculated by summation of the products of the template values with the corresponding input pixel values $\gamma(k, l)$, i.e.,

$$G_2(i, j) = \sum_{k=i-2}^{i+2} \sum_{l=j-2}^{j+2} \tau\gamma(k,l), \qquad (12)$$

with τ also dependent on $\varsigma = |i - k| + |j - l|$:

$$\tau = \begin{cases} 1 \Leftrightarrow (\varsigma = 0) \vee (\varsigma = 4) \\ 2 \Leftrightarrow \varsigma = 3 \\ 3 \Leftrightarrow (\varsigma = 2) \wedge ((i = k) \vee (j = k)) \\ 4 \Leftrightarrow (\varsigma = 2) \wedge ((i \neq k) \wedge (j \neq k)) \\ 5 \Leftrightarrow \varsigma = 1 \end{cases}$$

where $\wedge$ denotes that both conditions should apply. The main difference between G_1 and G_2 is the incorporation in G_2 of pixels that are noncontiguous to the central pixel. Note that $1 \leq G_2(i, j) \leq 69$ and that large patches localized in each other's vicinity will generate the largest G_2 values.

[19] Finally, we measure the conditional probability P_c that, given a pixel of the class of interest, the nearest neighbor is also a pixel of the class of interest [*Riiters et al.*, 2000]. This measure is considered a measure of fragmentation and can be used as a variant of contiguity assessment. The main difference with G_1 and G_2 is that not only contiguity with the central input pixel is assessed but that all nearest neighborships in the template are weighted equally. Diagonally neighboring pixels are not considered as pixel pairs. P_c was assessed using four templates: 3×3, 5×5, 7×7, and 9×9. The templates do not contain weight factors but only delimit the vicinity in which pixel adjacencies are quantified. P_c is calculated as

$$P_c = \frac{n_2}{n_1}, \qquad (13)$$

with n_1 the number of pixel pairs that include at least one pixel of the class of interest and n_2 the number of pixel pairs of which both pixels belong to the class of interest. For each calculation in a $m \times m$ template, $2m(m - 1)$

Table 3. Coherence, Largest Patch Index, and Fragmentation[a]

PI	C	S	F
		Eurasia	
2	0.106	0.124	0.058
3	0.027	0.114	0.046
4	0.012	0.056	0.036
5	0.194	0.417	0.013
6	0.069	0.235	0.028
		North America	
2	0.031	0.104	0.056
3	0.039	0.133	0.031
4	0.026	0.08	0.030
5	0.078	0.207	0.020
6	0.039	0.079	0.040

[a] Coherence (C), largest patch index (S), and fragmentation (F) for persistence index (PI) data in Eurasia and North America.
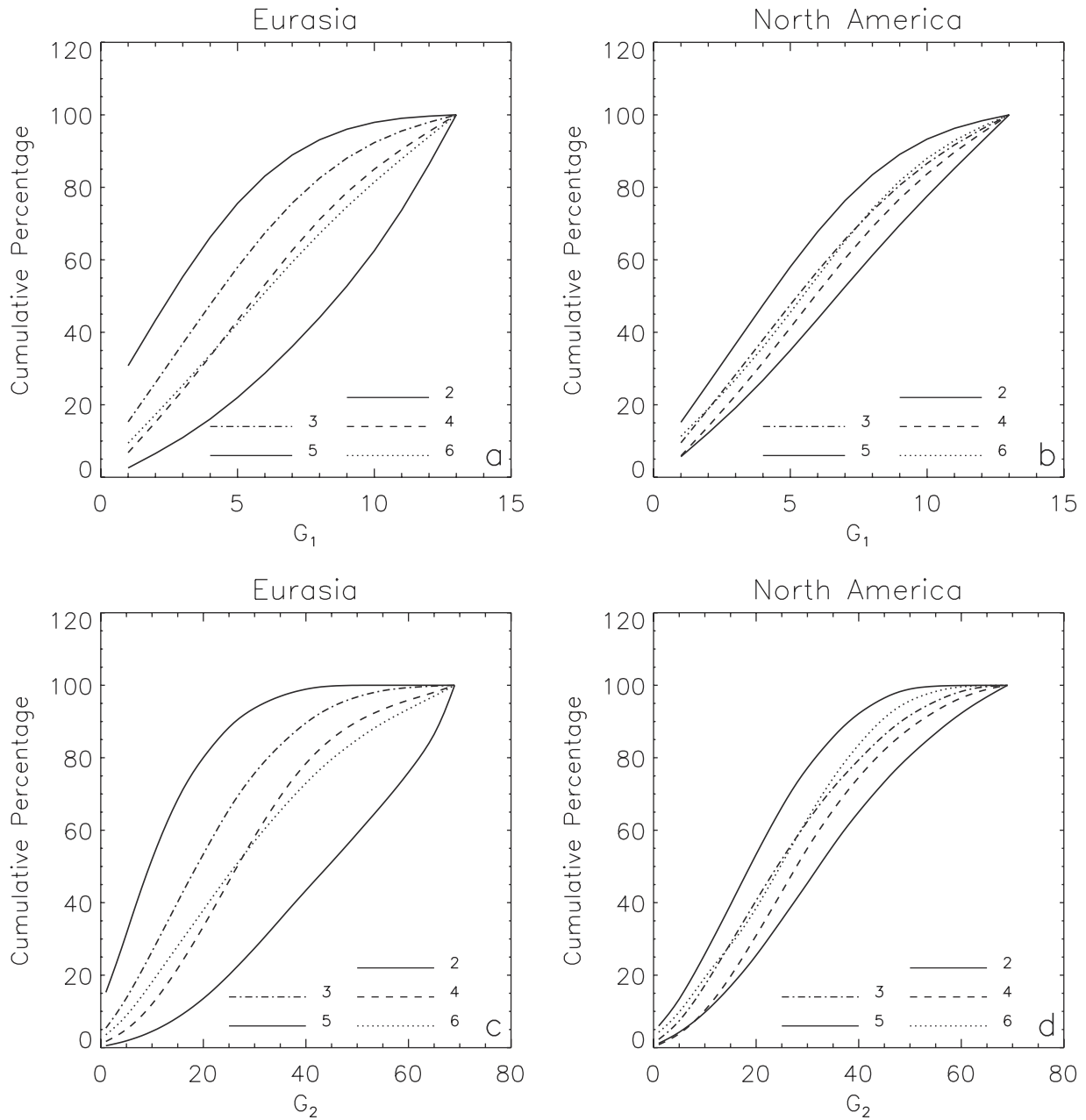
Figure 5. Pixel contiguity G_1 and clustering G_2 distribution: (a) cumulative contiguity value distribution for different persistence values ($PI = 2, 3, \ldots, 6$) in Eurasia; (b) cumulative contiguity value distribution for different persistence values ($PI = 2, 3, \ldots, 6$) in North America; (c) cumulative clustering value distribution for different persistence values ($PI = 2, 3, \ldots, 6$) in Eurasia; (d) cumulative clustering value distribution for different persistence values ($PI = 2, 3, \ldots, 6$) in North America.

pairs have to be considered. P_c equals zero if none of the pairs includes two pixels; P_c equals one if all pixels in the template are pixels of the class of interest. In the output image the value of P_c is given to the central pixel of the template.

[20] Note that G_1, G_2, and P_c are only evaluated if the central pixel of the template belongs to the class of interest; otherwise, a value of zero is assigned to the pixel in the output image corresponding to the template's central pixel. Because calculation of G_1, G_2, and P_c is an intermediate between a pixel-level analysis and a patch-level analysis (only pixel-to-pixel neighborships are con-

sidered; patch extent can exceed the template size or can fractionally intersect), the threshold of 9 pixels was not applied.

3.   Results and Discussion

3.1.   Patch Number, Area, and Perimeter

[21] The number of patches (n) increases with persistence level, peaks at a persistence index (PI) value of 4, and then decreases on both continents (Table 1). The peak values represent ~39 and 35% of the total patches in Eurasia and North America, respectively. The decline from

Table 4. Contiguity, Clustering, and Neighborship Probability Statistics[a]

PI	$\bar{G}_1$	C.V.	$\bar{G}_2$	C.V.	$\bar{P}_c$	C.V.	$\bar{P}_c$	C.V.
					3 × 3		9 × 9	
Eurasia								
2	3.47	0.70	12.10	0.81	0.17	1.11	0.14	0.80
3	5.00	0.60	21.01	0.66	0.28	0.86	0.24	0.62
4	6.36	0.51	28.64	0.54	0.38	0.71	0.34	0.53
5	8.85	0.40	43.42	0.43	0.60	0.52	0.55	0.44
6	6.55	0.55	28.89	0.63	0.41	0.72	0.37	0.58
North America								
2	4.95	0.59	20.40	0.62	0.28	0.84	0.23	0.56
3	5.97	0.55	26.38	0.58	0.36	0.75	0.31	0.55
4	6.54	0.50	29.92	0.52	0.40	0.69	0.35	0.50
5	7.23	0.48	33.60	0.51	0.46	0.64	0.41	0.49
6	5.99	0.53	25.27	0.57	0.37	0.68	0.32	0.47

[a] Mean contiguity (G_1), mean clustering ($\bar{G}_2$), and mean conditional probability of neighborship ($\bar{P}_c$) for persistence index (PI) data in Eurasia and North America. Each statistic precedes its coefficient of variation (C.V.). P_c results are listed only for a 3 × 3 and 9 × 9 template. Several value pairs are statistically not different at the 0.05 level. For $\bar{G}_1$, value pairs (5.00; 4.95), (6.55; 6.54), and (5.97; 5.99). For $\bar{G}_2$, value pairs (21.01; 20.40) and (28.64; 28.89). For P_c with a 3 × 3 template, value pair (0.36; 0.37). For P_c with a 9 × 9 template, value pairs (0.24; 0.23) and (0.31; 0.32).

this value is different on the two continents. For instance, patches of $PI = 5$ ($PI = 2$) are ∼34 and 24% (1 and 12%) of the total patches in Eurasia and North America, respectively. Thus there are relatively more (fewer) patches in Eurasia at high (low) persistence levels compared to North America. This is indicative of a more persistent greening in Eurasia.

[22] The largest total patch area (a_t) is observed for $PI = 5$ on both continents. However, in Eurasia this represents 60% of the total area, while it is only 37% in North America. The NDVI trend was therefore less persistent over a larger area in North America than in Eurasia, proportionally. In fact, for $PI \leq 3$ the absolute area in North America even exceeds that of Eurasia despite its smaller areal extent. This suggests high interannual variability in North American NDVI changes; i.e., the trend is not consistent with time that is characteristic of low persistence levels.

[23] The mean patch size ($\bar{a}$) increases with increasing persistence level, up to $PI = 5$. The decrease at $PI = 6$ is to be expected in view of a global cooling trend following the eruption of Mount Pinatubo in June 1991 (cf. Figure 1a). This decrease is observed for a_t and also for several other indices. A related metric, the patch density ($n/a_t = (\bar{a})^{-1}$), which is a measure of spatial "scattering" or fragmentation, likewise decreases with increasing persistence level, and is higher (lower) in Eurasia than in North America at low (high) persistence levels. Thus regions showing a persistent increase in NDVI are relatively more fragmented in North America.

[24] The cumulative distribution of patch sizes is shown in Figures 4a and 4b for different persistence levels. The contribution of large patches to the total patch area increases with persistence level, up to $PI = 5$. For $PI > 5$ a decrease is observed (cf. Table 1), which is more pronounced in North America, compared to Eurasia. The presence of large patches signifies an identical trend in many vicinal pixels. Correspondingly, smaller patches are indicative of a more fragmented pattern. At low persistence levels ($PI \leq 4$) a larger fraction of the area is associated with large patches in North America relative to Eurasia. The opposite is the case at higher persistence levels, where for $PI = 5$, fully 60% (50%) of the area is present in these large patches in Eurasia

(North America). Thus a larger fraction of the region exhibiting consistent greening is situated in large patches in Eurasia. In North America the same is true, but of regions exhibiting a short-term trend.

[25] The tendencies seen in patch size distributions are reflected by the size of the largest patch (a_{max}), which increases from $PI = 2$ to 5 (Table 1). This affects patch size variation, as expressed by the coefficient of variation, defined as the ratio of the standard deviation to the mean value (C.V., henceforth), which peaks at $PI = 5$ in both continents, more notably in Eurasia. The C.V. decreases clearly if only small patches of a comparable size are present, as in the case of $PI = 2$. The larger C.V. values at high persistence levels in Eurasia indicate an aggregated pattern formed from a mixture of large and small patches.

[26] The total patch perimeter p_t values increase with persistence level, up to $PI = 4$ in North America and $PI = 5$ in Eurasia and decrease thereafter (Table 2). The average perimeter $\bar{p}$ likewise increases up to $PI = 5$ and then decreases. Elongated patches are characterized by large perimeter lengths and compact patches by small perimeter lengths. Patches of low (high) persistence have higher (lower) perimeters in North America relative to Eurasia. This is consistent with observations of patch areas. Perimeter values generally increase with area because minimum perimeter lengths are associated with given area values in raster data [*Bribiesca*, 1997; *Bogaert et al.*, 2000a].

[27] The fraction of total perimeter taken by different perimeter length values is shown in Figures 4c and 4d. A general increase of the fraction of large perimeter lengths with increasing persistence is observed on both continents, up to $PI \leq 5$. At low persistence levels ($PI \leq 4$), patches in North America are more elongated, while at higher persistence levels Eurasian patches show extended perimeters. Alike for the patch size distribution (cf. Figures 4a and 4b), for $PI = 6$, lower values are observed, where North America shows a larger fraction of smaller perimeter values than Eurasia. The increase in perimeter lengths with persistence can also be seen in p_{max} results (Table 2). The presence of longer perimeters mixed with smaller lengths is confirmed by the C.V. The highest value is in layer $PI = 5$ in Eurasia; in North America this is less clear.
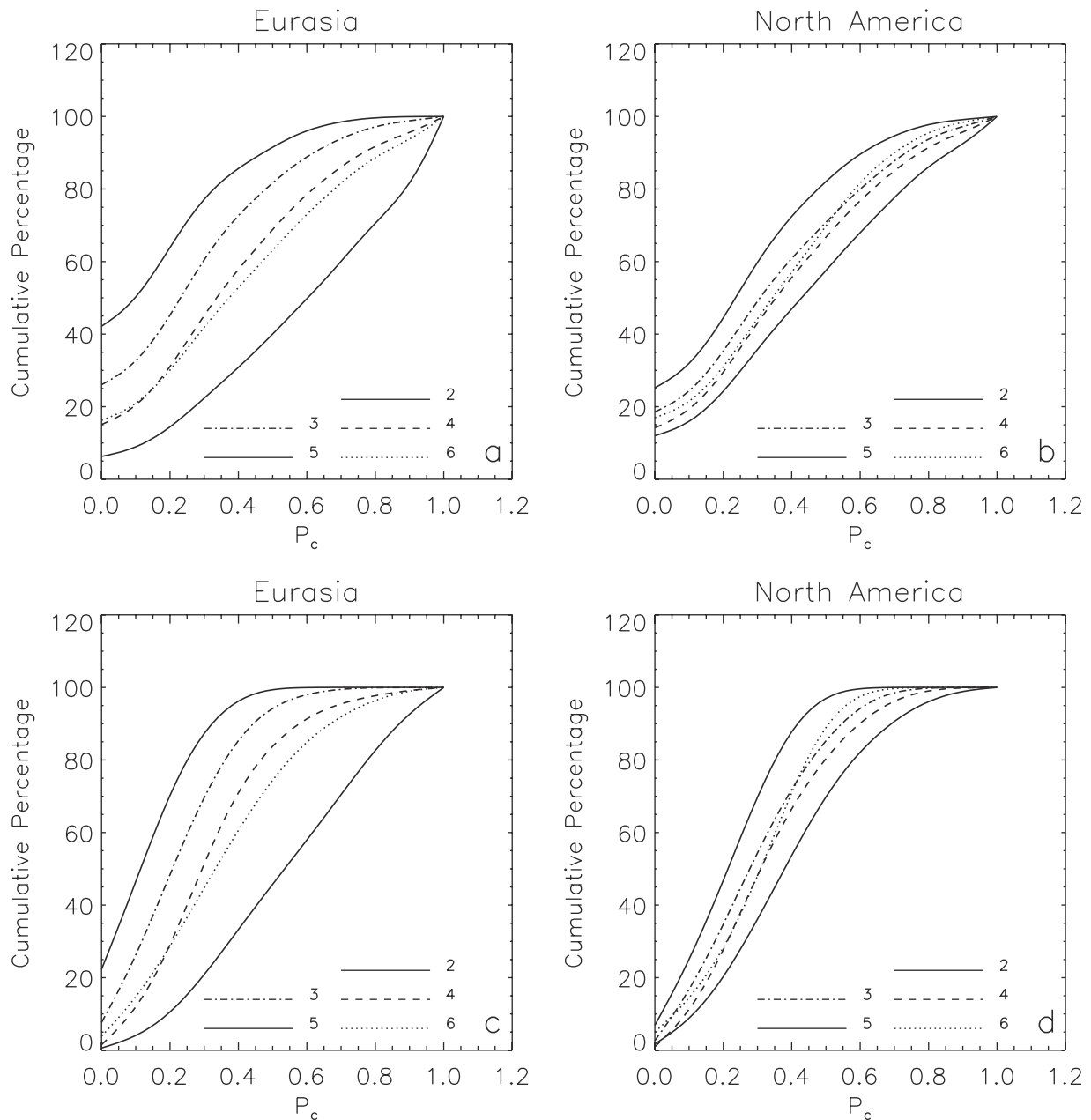
Figure 6. Cumulative distribution of the conditional probability of neighborhood (P_c) for different persistence values ($PI = 2, 3, \ldots, 6$): (a) Eurasia, using a 3×3 template; (b) North America, using a 3×3 template; (c) Eurasia, using a 9×9 template; (d) North America, using a 9×9 template.

Overall, these results suggest increasing perimeters with higher persistence level, and patches with extended perimeters at high persistence levels in Eurasia.

3.2. Coherence, Largest Patch Index, and Fragmentation

[28] Coherence (C) is preferably evaluated using the reference value for the case of perfect evenness ($= n^{-1}$). Although all coherence values exceed the reference value, three data layers in particular show a clear deviation from perfect evenness (Table 3). Coherence is ~50 times the reference value for $PI = 5$ (~7 times for $PI = 6$) in Eurasia

clearly indicating dominance of a few large patches. The corresponding coherence value in North America is only ~8 times the reference value and reflects a less aggregated pattern. This is consistent with observations of patch size distribution (Figures 4a and 4b), a_{max}, and the C.V. (Table 1). Note that the relatively high coherence value of the $PI = 2$ layer in Eurasia ($C = 0.106$) is an artefact of too few patches ($n = 10$).

[29] The largest patch index (S) reveals that the $PI = 5$ layers are especially dominated by a large patch, which in Eurasia occupies about 42% of a_t (Table 3). A large patch is also seen in Eurasia for $PI = 6$ ($S = 0.235$), but not in North America ($S = 0.079$). The S values are comparable for the two

Table 5. Lorenz Curve Lengths for Spatial Pattern Metrics[a]

Index	L		$\Delta\%$
	Eurasia	North America	
n	1.508	1.450	+4.00
a_t	1.571	1.489	+5.51
$\bar{a}$	1.474	1.439	+2.43
a_{max}	1.691	1.538	+9.95
p_t	1.541	1.474	+4.55
$\bar{p}$	1.438	1.425	+0.91
p_{max}	1.663	1.497	+11.09
C	1.518	1.441	+5.34
S	1.484	1.438	+3.20
F	1.450	1.434	+1.12
$\bar{G}_1$	1.430	1.417	+0.92
$\bar{G}_2$	1.441	1.419	+1.55
$\bar{P}_c$ 3×3	1.441	1.419	+1.55
$\bar{P}_c$ 9×9	1.445	1.420	+1.76

[a] Lorenz curve lengths (L) for persistence index data in Eurasia and North America, where L is calculated for patch number (n), total patch area (a_t), mean patch area ($\bar{a}$), maximum patch area (a_{max}), total patch perimeter (p_t), mean patch perimeter ($\bar{p}$), maximum patch perimeter (p_{max}), coherence (C), largest patch index (S), fragmentation (F), mean contiguity ($\bar{G}_1$), mean clustering ($\bar{G}_2$), and mean conditional probability of neighborship ($\bar{P}_c$) for both the 3×3 and 9×9 template. $\Delta\%$ equals the relative difference between both values.

continents at low persistence levels. The low values for $PI = 4$ layers are associated with high patch numbers (cf. Table 1) which leads to patch size evenness, as confirmed by C.

[30] The fragmentation index F should be evaluated by taking into account the minimum number of pixels per patch (which is nine) and expressed relative to F_{max} (Table 3). The index decreases with increasing persistence, up to $PI = 5$, and increases again. The low F values for $PI = 5$ ($F = 0.013$ and 0.020 for Eurasia and North America, respectively) indicate a tendency for pixel aggregation, which is also reflected by the larger clusters in this layer, as previously described (section 3.1). In general, all data layers show low F values, but the $PI = 2$ layer shows a degree of fragmentation exceeding 50% of F_{max}. One can also note that in Eurasia low persistence patches ($PI < 5$) show higher fragmentation and high persistence patches show higher aggregation, as compared to North America.

3.3. Contiguity, Clustering, and Neighborhood Probability

[31] Mean contiguity ($\bar{G}_1$) increases with increasing persistence level up to $PI = 5$ and then decreases (Table 4), thus establishing a general relation between persistence and connectedness. Low C.V. values are seen in the $PI = 5$ layers, which indicates a more homogeneous spatial structure characterized by a high degree of connectedness. The mean values for North America exceed those of Eurasia only at low persistence levels ($PI \leq 4$). Thus, on the basis of neighborships, Eurasia shows a less fragmented pattern than North America at high persistence levels. The cumulative percentage of pixel contiguity values also shows the largest proportion of high G_1 values for $PI = 5$ (Figures 5a and 5b). This increasing fraction of high G_1 values with persistence level is reflected by the concave to convex change in the shape of the curves. The higher convexity of the Eurasian curves for $PI \geq 5$ thus reflects a higher degree of connectedness. All differences between the

average contiguity values are significant at the $p = 0.05$ level (Table 4), with the exception of three out of a total of 45; i.e., G_1 enables identification of the various persistence layers.

[32] The results for clustering G_2 are similar to those for contiguity (Table 4). Pixels with higher persistence exhibit higher values of mean clustering $\bar{G}_2$ and vice versa. Regions of low (high) persistence in Eurasia are less (more) clustered and more (less) spatially remote compared to North America. Because less clustering is typical of fragmented patterns, regions of high persistence are more fragmented in North America. The C.V. values reveal (1) maximum clustering heterogeneity for $PI = 2$, indicating patterns formed by mixtures of clustered and remote pixels (C.V. = 0.81 and 0.62 for Eurasia and North America, respectively) and, (2) minimum C.V. values for $PI = 5$ generated by dominance of high G_2 values representing an overall (homogeneous) clustered pattern (C.V. = 0.43 and 0.51). The $\bar{G}_2$ values are significantly different (Table 4, $p = 0.05$), with the exception of two out of a total of 45 tests. Thus every layer is characterized by a particular degree of clustering. The increase in clustering with persistence level is also reflected by the concave to convex change in the shape of the pixel distribution (Figures 5c and 5d). The most convex distribution represents the most clustered layer, and this is in Eurasia, $PI = 5$.

[33] Assessment of conditional neighborhood probabilities P_c further confirms contiguity and clustering results. The probability of finding an adjacent pixel is highest for the $PI = 5$ layer (Table 4). A stronger tendency for adjacency is observed in Eurasia at high persistence levels ($\bar{P}_c = 0.60$ and $\bar{P}_c = 0.55$ versus $\bar{P}_c = 0.46$ and $\bar{P}_c = 0.41$, for the 3×3 and 9×9 templates, respectively). North America shows higher connectedness at low persistence values. The cumulative percentages of pixel probabilities for both templates are shown in Figure 6. A tendency for convexity in the shape of this distribution with increasing persistence values indicates a higher probability of patch formation and connectedness. The curves, especially those for Eurasia, clearly indicate differences in the underlying spatial patterns, which are characteristic of pixel scattering in the case of $PI = 2$ and adjacency in the case of $PI = 5$. Overall, the $PI = 5$ layer in Eurasia remains the least heterogeneous (C.V. = 0.52 and 0.44 for the 3×3 and the 9×9 template, respectively). Note that increasing the template dimensions does decrease the number of low

Table 6. Lorenz Curve Lengths for the Coefficient of Variation of the Spatial Pattern Metrics[a]

Index	L		$\Delta\%$
	Eurasia	North America	
a	1.533	1.451	+5.65
p	1.528	1.442	+5.95
G_1	1.420	1.415	+0.35
G_2	1.422	1.415	+0.50
P_c 3×3	1.425	1.416	+0.64
P_c 9×9	1.421	1.415	+0.42

[a] Lorenz curve lengths (L) for persistence index data in Eurasia and North America, where L is calculated for the coefficient of variation (C.V.) of patch area (a), patch perimeter (p), contiguity (G_1), clustering (G_2), and conditional probability of neighborship (P_c) for both the 3×3 and 9×9 template. $\Delta\%$ equals the relative difference between both values.

P_c values because of higher probability of finding pixel pairs within a larger window. However, this does not increase the overall P_c value, as evidenced by decreasing $\bar{P}_c$ from 3×3 to 9×9, probably owing to detection of extra pixel pairs containing not more than a single pixel. Inclusion of one spatially isolated pair containing two pixels each can often generate additional detection of six pairs containing only one pixel. Also note that only one (two) statistically insignificant difference is (are) observed for $\bar{P}_c$ for the 3×3 (9×9) template (Table 4).

[34] It should be emphasized that patches with $PI = 5$ in both Eurasia and North America exhibit a pattern statistically different from all other data layers, as measured by $\bar{G}_1$, $\bar{G}_2$, and $\bar{P}_c$. Thus we conclude that the persistence index is a suitable measure of sustained NDVI increase.

3.4. Variation in Index Values

[35] The Lorenz curve lengths L for the aforementioned pattern indices are given in Table 5. No crossing Lorenz curves were observed, which is the basic condition for comparison of these curves. Low values of L indicate that the corresponding metric poorly discriminates the different persistence layers. High L values reflect large differences in pattern metric outcomes and hence signify spatial features that clearly change within the observed duration of NDVI increase. Note that L does not take into account the absolute values of the original data.

[36] The values of L for Eurasia always exceed those of North America, which reflects higher unevenness among the index outcomes for this continent. Thus the differences in spatial pattern between data sets representing different persistence levels are more pronounced in Eurasia than in North America.

[37] The largest L values are noted for a_{max} and p_{max} (1.691 and 1.663, generating differences of 10 and 11%, respectively), because these indices describe an extreme feature of the spatial pattern. Intermediate differences are noted for n, a_t, p_t, and C. Measures based only on pixel patterns, without accounting for variability in pixel size, i.e., F, $\bar{G}_1$, $\bar{G}_2$, and $\bar{P}_c$, show less variation between persistence levels. The inclusion of spatially isolated pixels and clusters, fewer than 9 pixels, is the probable cause of higher evenness in $\bar{G}_1$, $\bar{G}_2$, and $\bar{P}_c$ outcomes. The intermediate statistic for n confirms this. The major structural difference between layers of different persistence is therefore associated with the occurrence of large pixel clusters. This is quantified adequately by a_{max} and p_{max}, features of the largest patch(es) in the data.

[38] The Lorenz curve lengths can also be evaluated for the coefficients of variation of the different metrics (Table 6). Analogously, the L values of a and p, i.e., those based on patch data, show higher differences in evenness between Eurasia and North America than those solely based upon pixel data (G_1, G_2, and P_c).

[39] The differences in structural homogeneity between the Eurasian data layers are more marked than those of North America. Hence, in addition to changes in the spatial structure, the internal homogeneity of the layer also changes with persistence level. Finally, it should be noted that spatial metrics F, G_1, G_2, and P_c hardly discriminate the North American data layers, as reflected by L values close to the minimum, $L = \sqrt{2}$. However, this evenness does not imply statistically insignificant differences in spatial structure (cf. section 3.3).

4. Summary and Conclusions

[40] A recent analysis suggests not only a strong correlation between satellite vegetation index and station temperature data, but also a more persistent greening trend in Eurasia relative to North America, for the period 1982 to 1999 [*Zhou et al.*, 2001]. In view of the linkage between NDVI data and vegetation photosynthetic activity [*Keeling et al.*, 1996; *Myneni et al.*, 1997; *Randerson et al.*, 1999], this inference requires a more rigorous elaboration than that presented in *Zhou et al.* [2001].

[41] *Zhou et al.* [2001] characterized the greening trend recorded in the satellite data, in the 40°N–70°N band, in terms of a persistence index, which identified locations where the NDVI had increased consistently during the 1981 to 1999 time period. We examine the spatial structure of data layers associated with various persistence levels to enquire (1) if an increase in persistence index value is characteristic of a consistent long-term greening trend and (2) if the spatial patterns of vegetation index changes are different between Eurasia and North America. Because the persistence index is calculated on a per pixel basis, spatial information (pixel vicinity) is retained, and patches composed of adjacent pixels of identical persistence value will determine the spatial structure of the greening trend.

[42] The selection of metrics suitable for assessment of spatial patterns is subject to debate. The use of multiple indices, necessary because of pattern complexity, is mortgaged by index redundancy [*Riiters et al.*, 1995; *Haines-Young and Chopping*, 1996]. The selection of indices should, however, be guided by the goals of the investigation. In our case we selected landscape indices characteristic of fragmentation and connectedness. Indices based on convolving a pixel mask with binary digital images were used to complement indices generating a single value for the entire image. In addition to mean and variance analysis, the latter for assessment of spatial homogeneity, we used Lorenz curve length statistics to evaluate internal variability of metric outcomes.

[43] Regions of high NDVI persistence values in Eurasia exhibit higher connectivity with large dominant patches, lower patch density, higher patch coherence, more pixel clustering, more contiguous pixels, more aggregation, and a higher probability of finding orthogonal neighbors. In North America the spatial pattern of long-term NDVI increases is fragmented with a higher patch density, smaller patches, a few large connected regions, less coherence, and higher values of the fragmentation index. The template statistics confirm this tendency for less connectedness, pixel remoteness, and a lower probability of finding an orthogonal neighbor. It is thus we infer a persistent and spatially extensive greening trend in Eurasia since the early 1980s. Finally, we note that the spatial analysis reported here convincingly demonstrates the utility of the persistence index for characterizing a sustained long-term increase in NDVI.

References

Antrop, M., The language of landscape ecologists and planners—A comparative content analysis of concepts used in landscape ecology, *Landscape Urban Plan.*, *55*, 163–173, 2001.

Asrar, G., M. Fuchs, E. T. Kanemasu, and J. L. Hatfield, Estimating absorbed photosynthetic radiation and leaf area index from spectral reflectance in wheat, *Agron. J.*, *76*, 300–306, 1984.

Bogaert, J., P. Van Hecke, R. Moermans, and I. Impens, Twist number statistics as an additional measure of habitat perimeter irregularity, *Environ. Ecol. Stat.*, *6*, 275–290, 1999.

Bogaert, J., R. Rousseau, P. Van Hecke, and I. Impens, Alternative area-perimeter relations for measurement of 2-D shape compactness of habitats, *Appl. Math. Comput.*, *111*, 71–85, 2000a.

Bogaert, J., R. Rousseau, P. Van Hecke, D. Salvador-Van Eysenrode, and R. Ceulemans, The Lorenz curve as an indicator of scale effect on image information content, in *Quantitative Approaches to Landscape Ecology*, edited by T. Clare and D. Howard, pp. 121–129, IALE(UK), Bangor, UK, 2000b.

Bogaert, J., P. Van Hecke, D. Salvador-Van Eysenrode, and I. Impens, Landscape fragmentation assessment using a single measure, *Wildlife Soc. B.*, *28*, 875–881, 2000c.

Bogaert, J., D. Salvador-Van Eysenrode, I. Impens, and P. Van Hecke, The interior-to-edge breakpoint distance as a guideline for nature conservation policy, *Environ. Manage.*, *27*, 493–500, 2001.

Bradley, N. L., A. C. Leopold, J. Ross, and W. Huffaker, Phenological changes reflect climate change in Wisconsin, *Proc. Natl. Acad. Sci. USA*, *96*, 9701–9704, 1999.

Bribiesca, E., Measuring 2-D shape compactness using the contact perimeter, *Comput. Math. Appl.*, *33*, 1–9, 1997.

Brown, J. L., S.-H. Li, and N. Bhagabati, Long-term trend toward earlier breeding in an American bird: a response to global warming, *Proc. Natl. Acad. Sci. USA*, *96*, 5565–5569, 1999.

Cain, D. H., K. H. Riiters, and K. Orvis, A multi-scale analysis of landscape statistics, *Landscape Ecol.*, *12*, 199–212, 1997.

Cayan, R. C., S.A. Kammerdiener, M. D. Dettinger, J. M. Caprio, and D. H. Peterson, Changes in the onset of spring in the western United States, *Bull. Am. Meteorol. Soc.*, *82*, 399–415, 2001.

Colombo, S. J., Climatic warming and its effect on bud burst and risk of frost damage to white spruce in Canada, *Forest. Chron.*, *74*, 567–577, 1998.

Crick, H. Q. P., and T. H. Sparks, Climate change related to egg-laying trends, *Nature*, *399*, 423–424, 1999.

Crick, H. Q. P., C. Dudley, D. E. Glue, and D. L. Thomson, UK birds are laying eggs earlier, *Nature*, *388*, 526, 1997.

Fitzjarrald, D. R., O. C. Acevedo, and K. E. Moore, Climatic consequences of leaf presence in the eastern United States, *J. Clim.*, *14*, 598–614, 2001.

Fortin, M.-J., Spatial statistics in landscape ecology, in *Landscape Ecological Analysis: Issues and Applications*, edited by J. M. Klopatek and R. H. Gardner, pp. 253–279, Springer-Verlag, New York, 1999.

Giles, R. H., and M. K. Trani, Key elements of landscape pattern measures, *Environ. Manage.*, *23*, 477–481, 1999.

Gustafson, E. J., Quantifying landscape spatial pattern: what is the state of the art, *Ecosystems*, *1*, 143–156, 1998.

Haines-Young, R., and M. Chopping, Quantifying landscape structure: a review of landscape indices and their applications to forested landscapes, *Prog. Phys. Geogr.*, *20*, 418–445, 1996.

Hansen, J., R. Ruedy, J. Glascoe, and M. Sato, GISS analysis of surface temperature change, *J. Geophys. Res.*, *104*, 30,997–31,022, 1999.

Hargis, C. D., J. A. Bissonette, and J. L. David, The behavior of landscape metrics commonly used in the study of habitat fragmentation, *Landscape Ecol.*, *19*, 167–186, 1998.

He, H. S., B. E. DeZonia, and D. J. Mladenoff, An aggregation index (AI) to quantify spatial patterns of landscapes, *Landscape Ecol.*, *15*, 591–601, 2000.

Herzog, F., A. Lausch, E. Müller, H.-H. Thulke, U. Steinhart, and S. Lehmann, Landscape metrics for assessment of landscape destruction and rehabilitation, *Environ. Manage.*, *27*, 91–107, 2001.

Holben, B. N., Characteristics of maximum value compositing images for AVHRR data, *Int. J. Remote Sens.*, *7*, 1417–1437, 1986.

Jaeger, J. A. G., Landscape division, splitting index, and effective mesh size: new measures of landscape fragmentation, *Landscape Ecol.*, *15*, 115–130, 2000.

Johnsson, K., Fragmentation index as a region based GIS operator, *Int. J. Geogr. Inf. Syst.*, *9*, 211–220, 1995.

Kaufmann, R. K., L. Zhou, Y. Knyazikhin, N. V. Shabanov, R. B. Myneni, and C. J. Tucker, Effect of orbital drift and sensor changes on the time series of AVHRR vegetation index data, *IEEE Trans. Geosci. Remote*, *38*, 2584–2597, 2000.

Keeling, C. D., J. F. S. Chin, and T. P. Whorf, Increased activity of northern vegetation inferred from atmospheric CO_2 measurements, *Nature*, *382*, 146–149, 1996.

Krummel, J. R., R. H. Gardner, G. Suguhara, R. V. O'Neill, and P. R. Coleman, Landscape patterns in a disturbed environment, *Oikos*, *48*, 321–324, 1987.

LaGro, J., Assessing patch shape in landscape mosaics, *Photogramm. Eng. Remote Sens.*, *57*, 285–293, 1991.

Li, H., and J. F. Reynolds, A simulation experiment to quantify spatial heterogeneity in categorical maps, *Ecology*, *75*, 2446–2455, 1994.

Lorenz, M. O., Methods of measuring concentration of wealth, *J. Am. Stat. Assoc.*, *9*, 209–219, 1905.

Los, S. O., Estimation of the ratio of sensor degradation between NOAA AVHRR channels 1 and 2 from monthly NDVI composites, *IEEE Trans. Geosci. Remote*, *36*, 202–213, 1998.

Los, S. O., C. O. Justice, and C. J. Tucker, A global $1° \times 1°$ NDVI data set for climate studies derived from the GIMMS continental NDVI data, *Int. J. Remote Sens.*, *15*, 3493–3518, 1994.

McGarigal, K., and B. J. Marks, Fragstats: Spatial pattern analysis program for quantifying landscape structure, *Gen. Tech. Rep. PNW-GTR-351*, 122 pp., USDA Forest Serv., Pac. Northwest Res. Stat., Portland, Oreg, 1995.

Menzel, A., and P. Fabian, Growing season extended in Europe, *Nature*, *397*, 659, 1999.

Milne, B. T., Lessons from applying fractal models to landscape patterns, in *Quantitative Methods in Landscape Ecology*, edited by M. G. Turner and R. H. Gardner, pp. 199–235, Springer-Verlag, New York, 1991.

Myneni, R. B., F. G. Hall, P. J. Sellers, and A. L. Marshak, The interpretation of spectral vegetation indices, *IEEE Trans. Geosci. Remote*, *33*, 481–486, 1995.

Myneni, R. B., C. D. Keeling, C. J. Tucker, G. Asrar, and R. R. Nemani, Increased plant growth in the northern high latitudes from 1981 to 1991, *Nature*, *386*, 698–702, 1997.

O'Neill, R. V., et al., Indices of landscape pattern, *Landscape Ecol.*, *3*, 153–162, 1988.

O'Neill, R. V., K. H. Riiters, J. D. Wickham, and K. B. Jones, Landscape pattern metrics and regional assessment, *Ecosyst. Health*, *5*, 225–233, 1999.

Parmesan, C., et al., Poleward shifts in geographical ranges of butterfly species associated with regional warming, *Nature*, *399*, 579–583, 1999.

Randerson, J. T., C. B. Field, I. Y. Fung, and P. P. Tans, Increases in early season ecosystem uptake explain recent changes in the seasonal cycle of atmospheric CO_2 at high northern latitudes, *Geophys. Res. Lett.*, *26*, 2765–2769, 1999.

Riiters, K. H., R. V. O'Neill, C. T. Hunsaker, J. D. Wickham, D. H. Yankee, S. P. Timmins, K. B. Jones, and B. L. Jackson, A factor analysis of landscape pattern and structure metrics, *Landscape Ecol.*, *10*, 23–39, 1995.

Riiters, K. H., J. D. Wickham, R. V. O'Neill, K. B. Jones, and E. Smith, Global-scale patterns of forest fragmentation (on line). *Conserv. Ecol.*, *4*(2), pap. 3, 2000.

Ripple, W. J., G. A. Bradshaw, and T. A. Spies, Measuring forest landscape patterns in the Cascade Range of Oregon, USA, *Biol. Conserv.*, *57*, 73–88, 1991.

Rosborough, G. W., D. G. Baldwin, and W. J. Emery, Precise AVHRR image navigation, *IEEE Trans. Geosci. Remote*, *32*, 644–657, 1994.

Rousseau, R., P. Van Hecke, D. Nijssen, and J. Bogaert, The relationship between diversity profiles, evenness and species richness based on partial ordering, *Environ. Ecol. Stat.*, *6*, 211–223, 1999.

Schumaker, N. H., Using landscape indices to predict habitat connectivity, *Ecology*, *77*, 1210–1225, 1996.

Schwartz, M. D., Green-wave phenology, *Nature*, *394*, 839–840, 1998.

Stine, P. A., and C. T. Hunsaker, An introduction to uncertainty issues for spatial data used in ecological applications, in *Spatial Uncertainty in Ecology—Implications for Remote Sensing and GIS Applications*, edited by C. T. Hunsaker et al., pp. 91–107, Springer-Verlag, New York, 2001.

Taillie, C., Species equitability: a comparative approach, in *Ecological Diversity in Theory and Practice*, edited by J. F. Grassle, G. P. Patil, W. Smith, and C. Taillie, pp. 51–65, Int. Cooperative, Fairland, Md., 1979.

Thomas, C. D., and J. J. Lennon, Birds extend their ranges northwards, *Nature*, *399*, 213, 1999.

Tucker, C. J., J. R. G. Townshend, and T. E. Goff, African land cover classification using satellite data, *Science*, *227*, 369–375, 1985.

Tucker, C. J., I. Y. Fung, C. D. Keeling, and R. H. Gammon, The relationship between atmospheric CO_2 variations and a satellite-derived vegetation index, *Nature*, *319*, 195–199, 1986.

Turner, M. G., Landscape ecology: the effect of pattern on process, *Annu. Rev. Ecol. Syst.*, *20*, 171–197, 1989.

Vermote, E., and N. Z. El Saleous, Stratospheric aerosol perturbing effect on remote sensing of vegetation: Operational method for the correction of AVHRR composite NDVI, *SPIE Atmospheric Sens. Modeling*, *2311*, 19–29, 1994.

Vermote, E., and Y. J. Kaufman, Absolute calibration of AVHRR visible and near-infrared channels using ocean and cloud views, *Int. J. Remote Sens.*, *16*, 2317–2340, 1995.

Zhou, L., C. J. Tucker, R. K. Kaufmann, D. Slayback, N. V. Shabanov, and R. B. Myneni, Variations in northern vegetation activity inferred from satellite data of vegetation index during 1981 to 1999, *J. Geophys. Res.*, *106*, 20,069–20,083, 2001.

————————

J. Bogaert and R. Ceulemans, Department of Biology, University of Antwerp, Universiteitsplein 1, B-2610 Wilrijk, Belgium. (Jan.Bogaert@ua.ac.be)

R. B. Myneni and L. Zhou, Department of Geography, Boston University, 675 Commonwealth Avenue, Boston, MA 02215-1401, USA.

C. J. Tucker, Biospheric Sciences Branch, Code 923, NASA Goddard Space Flight Center, Greenbelt, MD 20771, USA.

Figure 2. Spatial presence of persistent NDVI increase in the northern latitudes. (a) Zones of long-term greening, characterized by five or six periods of growing season average NDVI increase. (b) Zones of short-term greening, characterized by less than five periods of growing season average NDVI increase. For spatial analysis, adjacent pixels representing an identical persistence index value are clustered into "patches."